RESEARCH ARTICLE

Conformal optical black hole for cavity

Qingtao Ba[1,2], Yangyang Zhou[1,2], Jue Li[1,2], Wen Xiao[1,2], Longfang Ye[1,2], Yineng Liu[1,2], Jin-hui Chen[1,2]* and Huanyang Chen[1,2]*

Abstract

Whispering-gallery-mode (WGM) cavity is important for exploring physics of strong light-matter interaction. Yet it suffers from the notorious radiation loss universally due to the light tunneling effect through the curved boundary. In this work, we propose and demonstrate an optical black hole (OBH) cavity based on transformation optics. The radiation loss of all WGMs in the ideal OBH cavity is completely inhibited by an infinite wide potential barrier. Besides, the WGM field in the OBH cladding is revealed to follow $1/r^\alpha$ decay rule based on conformal mapping, which is fundamentally different from the conventional Hankel-function distributions in a homogeneous cavity. Experimentally, a truncated OBH cavity is achieved based on the effective medium theory, and both the Q-factor enhancement and tightly confined WGM fields are measured in the microwave spectra which agree well with the theoretical results. The circular OBH cavity is further applied to the arbitrary-shaped cavities including single-core and multi-core structures with high-Q factor via the conformal mapping. The OBH cavity design strategy can be generalized to resonant modes of various wave systems, such as acoustic and elastic waves, and finds applications in energy harvesting and optoelectronics.

Keywords: Whispering-gallery-mode cavity, Optical black hole, Transformation optics

1 Introduction

Whispering-gallery-mode (WGM) cavity is an intriguing platform for intensely enhancing light-matter interaction, which lays the foundations for ultra-low threshold lasers [1, 2], ultra-sensitive sensing [3–5], nonlinear optics [6–8] and quantum photonics [9–11]. The conventional WGM cavity is composed of homogeneous materials with constant refractive index both in the core and cladding. The light field is confined in the cavity through the total internal reflection (TIR) and enhanced through constructive interference. The ultrahigh-Q factor has been realized in various dielectric WGM cavities with a large mode volume (V) and angular momentum [6, 7, 12–14]. Nevertheless, the intrinsic radiation loss in an open boundary cavity with finite dielectric constant is ubiquitous, due to the light tunneling in the curved surface from the analog of quantum mechanics [15–18]. This radiation loss is remarkably increased and becomes the dominant loss mechanism when the resonant wavelength is comparable to the geometry size of the cavities [19, 20]. There is relentless effort for optimizing the Q/V in optical cavities, which is of great importance in exploring the cavity quantum electrodynamics (QED) [19, 21, 22].

So far, various approaches have been proposed to manipulate the radiation loss and improve the Q-factor [16, 23–25]. For example, the plasmonic cavity [16, 26, 27] was constructed employing the strong optical-field localizations of metals, however, the intrinsic ohmic loss in the plasmonic platform is unavoidable. Alternatively, the radially anisotropic claddings were implemented to compress more energy into the core of cavity, resulting in tighter optical confinement and a substantially higher Q-factor [23]. Unfortunately, for natural materials the anisotropic parameters are still challenging to implement.

*Correspondence: jimchen@xmu.edu.cn; kenyon@xmu.edu.cn

[1] Institute of Electromagnetics and Acoustics and Department of Physics, College of Physical Science and Technology, Xiamen University, Xiamen 361005, China
Full list of author information is available at the end of the article

Transformation optics (TO) offers great versatility for manipulating light rays and electromagnetic fields with novel functionalities in inhomogeneous dielectric materials [28–33] and structured metallic objects [34–36]. Many fascinating optical structures designed by TO, enable light deflection and trapping to mimic the cosmology effects [37–44]. In this work, we utilize TO theory to construct a class of optical black hole (OBH) cavities, including the single-core and multi-core cavity. The WGM fields outside the core of circular OBH cavity are revealed to follow an unconventional $1/r^\alpha$ decay rule from conformal mapping. Employing the effective potential model, we strictly prove that the radiation loss of WGM in the ideal OBH cavity can be completely inhibited thus the radiation Q-factor is infinite. Experimentally, we demonstrate both the Q-factor enhancement and tight field confinement of the truncated OBH cavity compared with a homogeneous cavity in the microwave spectra. The circular OBH cavity is further applied to the arbitrary-shaped cavities including single-core and multi-core structures with high-Q factor via the conformal mapping. This work paves the way to surface field manipulation with conformal transformation, which can be generalized to resonant modes of various wave systems, such as acoustic and elastic waves, and finds applications in energy harvesting and optoelectronics.

2 Results and discussions

Let's start by reviewing the TIR at the planar interface between two dielectric media as shown in Fig. 1a, considering a light beam with incident angle θ_i impinging on the boundary from a denser medium (n_1). When θ_i is greater than the critical angle $\thet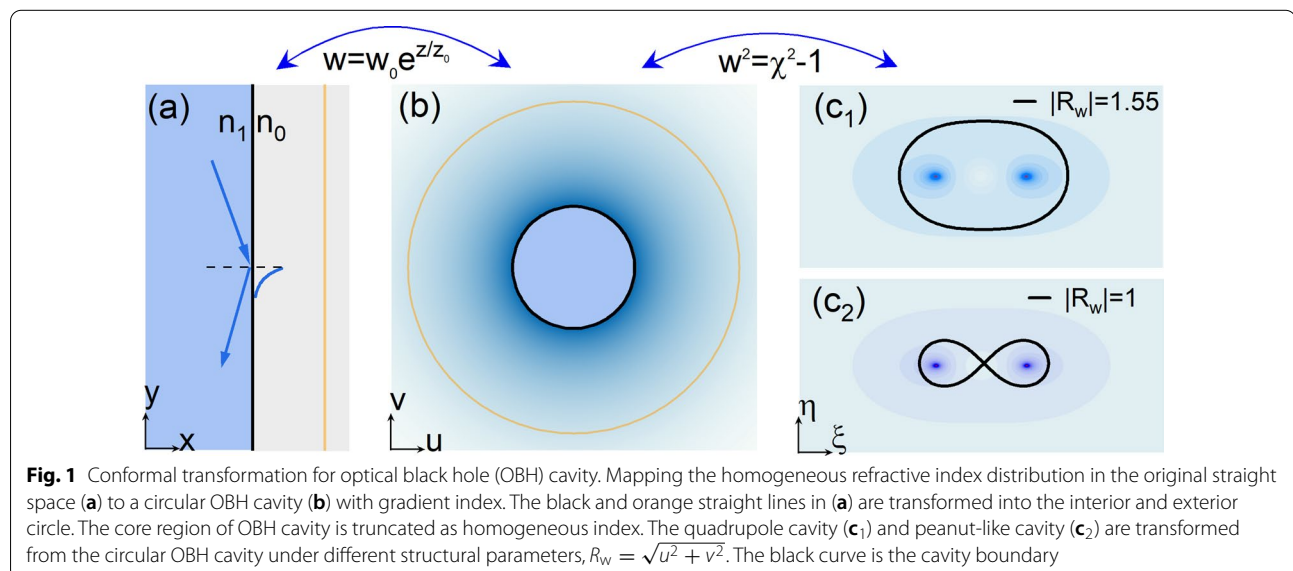a_c$ ($\theta_c = \arcsin(\frac{n_0}{n_1})$), only the decaying evanescent field exists in the less dense medium (n_0). Based on the TO theory, wave propagation in physical (z) space with homogeneous index (n_z) could be equivalent to that in the virtual (w) space with inhomogeneous index distribution. Thus, a two-dimensional (2D) OBH cavity in virtual space ($w = u + iv$) is constructed by implementing an exponential transformation: $w = w_0 e^{z/z_0}$ as shown in Fig. 1b, where $z = x + iy$ is complex variables of the physical space, w_0 and z_0 are the constants in w space and z space, respectively. The refractive index profile of OBH cavity is derived as:

$$n(r) = \begin{cases} n_z \left| \frac{dz}{dw} \right| = \frac{n_0}{r/R} & r > R \\ n_1 & r \le R \end{cases} \quad (1)$$

Note that we only conformally map the index distribution in the claddings ($r > R$) and keep the core region ($r \le R$) intact to avoid the divergence of index in the cavity center (see Additional file 1) [45]. As a consequence, the evanescent wave in w-space with polar coordinates can be obtained directly from the TIR-field transformation (see Additional file 1) [45]:

$$E(r, \varphi) = A \left(\frac{R}{r} \right)^\alpha e^{im_w \varphi} \quad (2)$$

where A is field amplitude, $\alpha = \sqrt{m_w^2 - (n_0 k_0 R)^2}$, $m_w = \beta R$, β and k_0 are the propagation wave vector in z-space and vacuum, respectively, and φ is the azimuthal angle. Therefore, the optical field in the cladding of the OBH cavity should follow the fast decay rule ($\sim 1/r^\alpha$), which is radically different from the Hankel-function distributions (asymptotic $\sqrt{1/r}$) of a homogeneous cavity. Further, a group of conformal OBH cavities, such as single-core and multi-core shapes, are engineered based

Fig. 1 Conformal transformation for optical black hole (OBH) cavity. Mapping the homogeneous refractive index distribution in the original straight space (**a**) to a circular OBH cavity (**b**) with gradient index. The black and orange straight lines in (**a**) are transformed into the interior and exterior circle. The core region of OBH cavity is truncated as homogeneous index. The quadrupole cavity (**c₁**) and peanut-like cavity (**c₂**) are transformed from the circular OBH cavity under different structural parameters, $R_w = \sqrt{u^2 + v^2}$. The black curve is the cavity boundary

on the form invariance of Maxwell's equations under coordinate transformations. Specifically, the mapping of $w^2 = \chi^2 - 1$ is performed on the circular OBH cavity [equation (1)], where $\chi = \xi + i\eta$, and the quadrupole (peanut-like) OBH cavity is constructed with $|R_w| = 1.55$ ($|R_w| = 1$) as shown in Fig. 1c₁ (Fig. 1c₂). The optical properties of these non-circular cavities are discussed later.

Now we analyze the WGM of a circular OBH cavity via the direct solution of Maxwell's equations in the cylindrical coordinates. Since the transverse electric (TE) and transverse magnetic (TM) polarizations are decoupled, we consider the TE polarization without the loss of generality. Employing the method of separating variables with the boundary continuity, the WGM fields in the cladding region of OBH cavity is derived (see Additional file 1) [45], which is nearly the same as equation (2). The eigen-equation of OBH cavity is as following:

$$k_0 n_1 R J'_m(n_1 k_0 R) = -\sqrt{m^2 - (n_0 k_0 R)^2} J_m(n_1 k_0 R) \quad (3)$$

where m is an integer, $J_m(n_1 k_0 R)$ is the m-order Bessel function. It is found that equation (3) has the real eigenvalue under certain conditions (see Additional file 1: Fig. S1) [45], which is completely different from the homogeneous cavity with complex eigenfrequency. Thus the radiation loss caused by the curved boundary is completely inhibited in OBH cavity [46].

The analytical results of WGM fields in OBH cavity are shown in Fig. 2a. Here, the structural parameters of circular OBH cavity are as following: $R = 3$ cm, $n_1 = 4$, $n_0 = 2$, which facilitates the experimental verification. In this study, only the lowest radial mode numbers are considered, due to their optical fields being closely confined to the cavity boundary and having the smallest radial extent. As a comparison, the WGM fields of a homogeneous cavity with the constant refractive index ($n'_1 = 4$, $n'_0 = 2$) is calculated as shown in Fig. 2b. The WGM fields in the OBH cavity are tightly confined near the boundary, by contrast, there is a considerable part of optical fields leaking into the cavity surroundings in the homogeneous cavity as shown in Fig. 2a, b (Additional file 1: Fig. S2) [45]. To quantitatively characterize the field confinement, we define a skin depth (SD) δ, i.e., the distance between the cavity boundary and the position with $1/e$ field-amplitude maximum. The SD of OBH cavity is always smaller than that of the homogeneous cavity as shown in Fig. 2c. Since the optical field confinement is enhanced with the increase of resonant mode number, SD is decreased with the mode number as well.

To more clearly elucidate the functions of the OBH refractive index profile, the radial cylindrical Bessel equation is modified as the analog of the Schrödinger
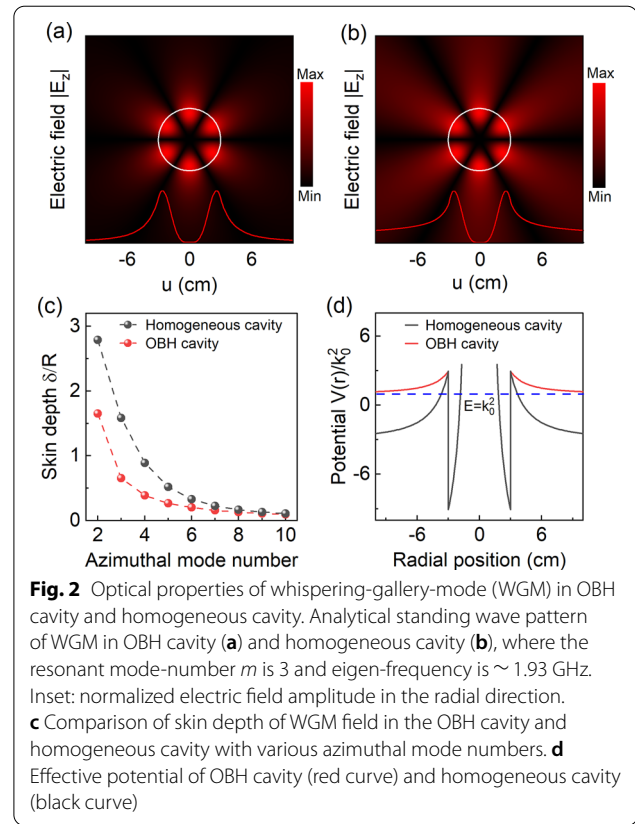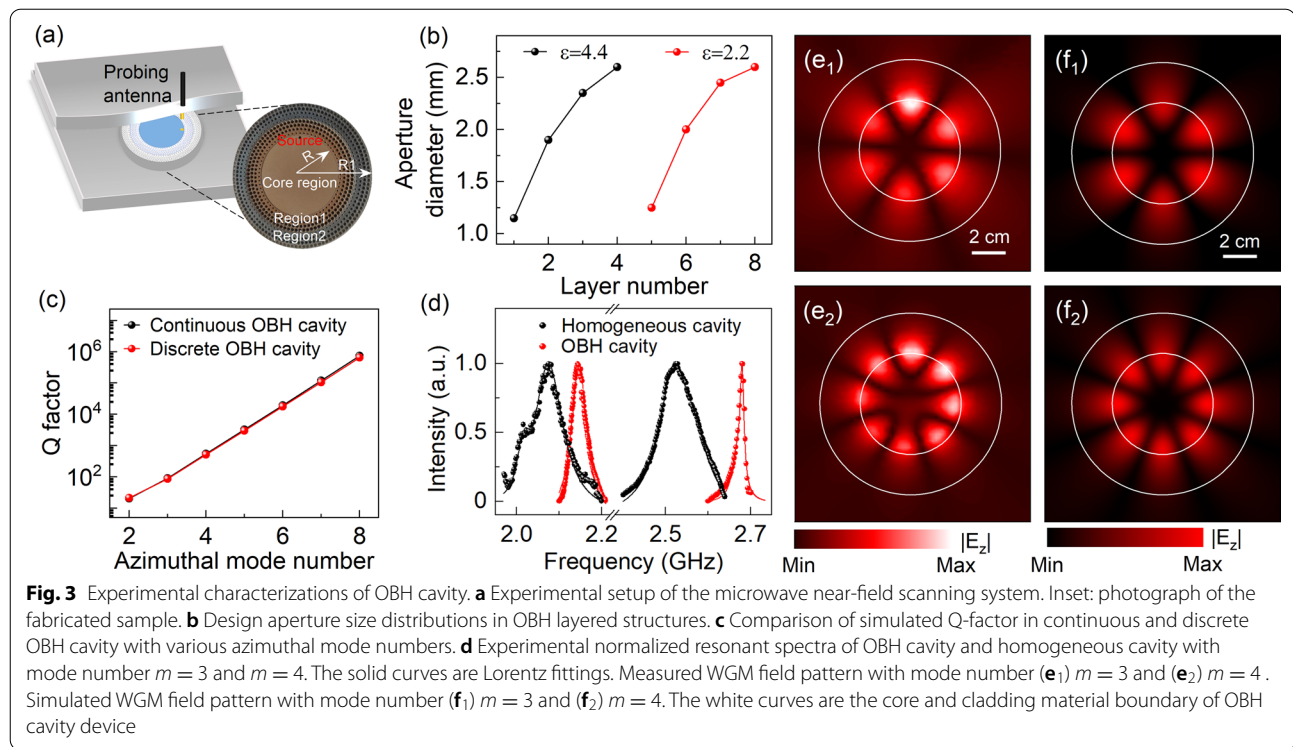

Fig. 2 Optical properties of whispering-gallery-mode (WGM) in OBH cavity and homogeneous cavity. Analytical standing wave pattern of WGM in OBH cavity (**a**) and homogeneous cavity (**b**), where the resonant mode-number m is 3 and eigen-frequency is ∼ 1.93 GHz. Inset: normalized electric field amplitude in the radial direction. **c** Comparison of skin depth of WGM field in the OBH cavity and homogeneous cavity with various azimuthal mode numbers. **d** Effective potential of OBH cavity (red curve) and homogeneous cavity (black curve)

equation [47]. The central potential function $V(r)$ of light propagation in OBH cavity is:

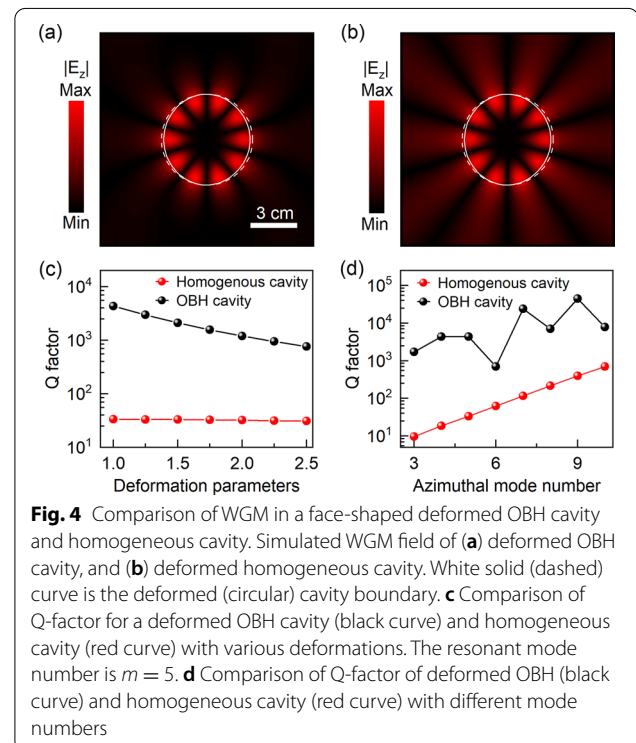$$V(r) = k_0^2[1 - n^2(r)] + \frac{(m + 1/2)(m - 1/2)}{r^2} \quad (4)$$

In particular, the potential function in the cladding region ($r > R$) is $V(r) = k_0^2 + (m^2 - n_0^2 k_0^2 R^2 - 1/4)/r^2$ as shown in Fig. 2d. Obviously, the OBH cladding relaxes the change of the potential barrier, and the eigen-energy (k_0^2) of WGM in OBH cavity is always smaller than the potential under the aforementioned cavity parameters. Thus, the WGM field is tightly confined within the potential well, and the classical radiation loss is completely inhibited theoretically. On the contrary, light always tunnels out of the open boundary in a homogeneous cavity since the eigen-energy of WGM is larger than the effective potential when $r \gg R$ (Fig. 2d black curve), and the radiation loss is not zero in all the WGMs. Note that in a conventional homogeneous cavity, the radiation loss predominates and the Q-factor is significantly decreased when the cavity geometry is comparable to the resonant wavelength (small resonant mode-number). Although an OBH cavity with a finite shell model has been theoretically studied to realize broadband light trapping/absorption and field penetration enhancement [15, 48], in this

Fig. 3 Experimental characterizations of OBH cavity. **a** Experimental setup of the microwave near-field scanning system. Inset: photograph of the fabricated sample. **b** Design aperture size distributions in OBH layered structures. **c** Comparison of simulated Q-factor in continuous and discrete OBH cavity with various azimuthal mode numbers. **d** Experimental normalized resonant spectra of OBH cavity and homogeneous cavity with mode number $m = 3$ and $m = 4$. The solid curves are Lorentz fittings. Measured WGM field pattern with mode number (e_1) $m = 3$ and (e_2) $m = 4$. Simulated WGM field pattern with mode number (f_1) $m = 3$ and (f_2) $m = 4$. The white curves are the core and cladding material boundary of OBH cavity device
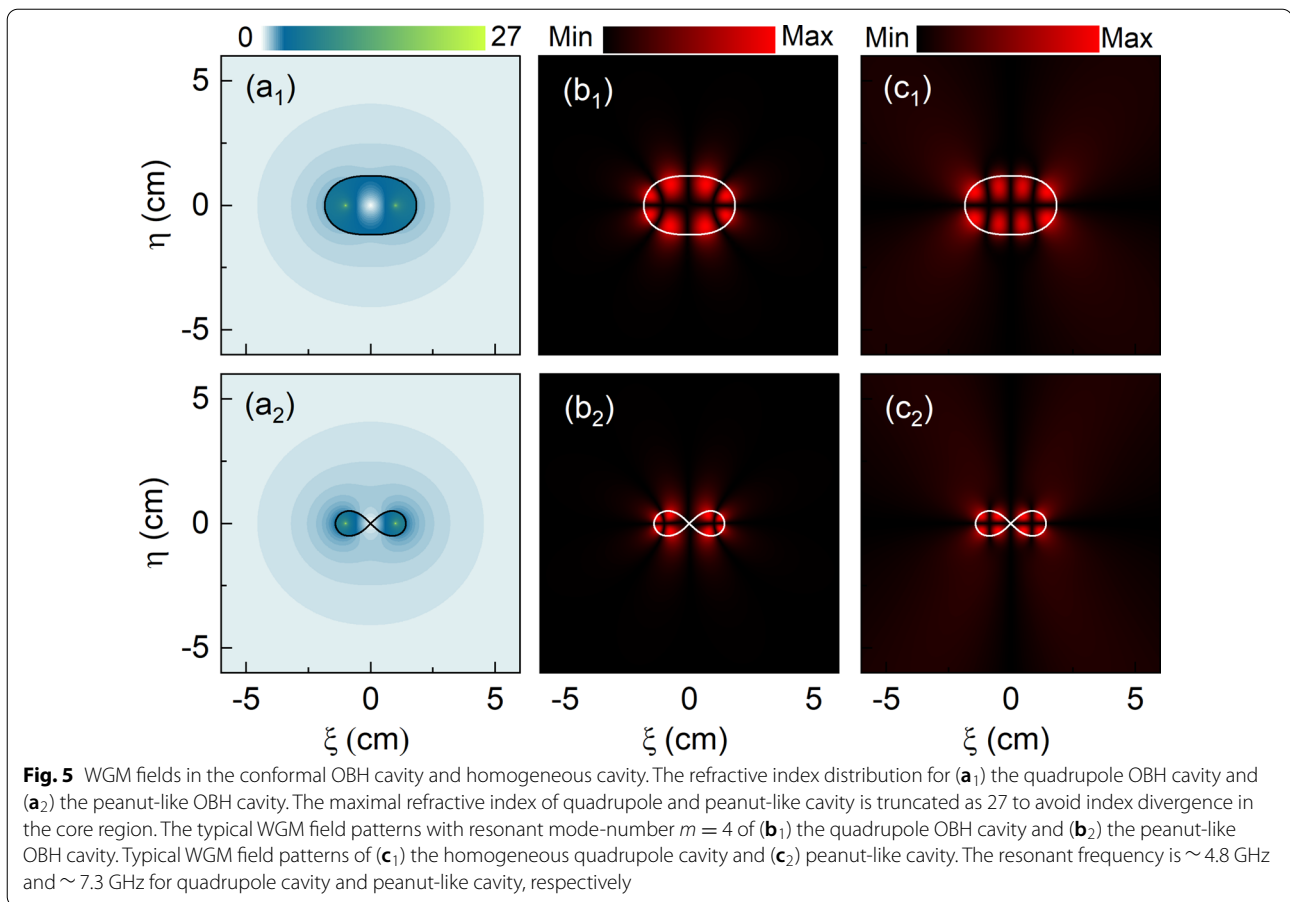
work we reveal the total radiation inhibition with infinite radiation Q-factor and the unique field decay rule in an ideal OBH cavity based on TO theory.

From Eq. (1), it demonstrates that a perfect OBH cavity requires an infinite region for gradient-index cladding that ranges from n_0 to 0. This is challenging to realize in conventional materials [37, 49–51]. Here, as an executable alternative, by truncating the area in the OBH cavity with an index of less than 1, we reserve the range of cladding index from n_0 to 1. Note that the index truncation breaks the ideal potential barrier and causes regenerated radiation loss (Additional file 1: Fig. S4) [45]. Nevertheless, the Q/S (S is the effective mode area for 2D cavities) enhancement of OBH cavity is still considerably high compared with a homogeneous cavity (Additional file 1: Fig. S5) [45]. Following that, the continuous OBH cladding is discretized into 9 layers with various effective index (Additional file 1: Fig. S6) [45], and the refractive index of the outermost layer ($r > 5.4$ cm) is simply set as air. Based on effective medium theory, the discrete layered index profile is achieved by drilling air holes with different diameters in two homogeneous dielectric slabs (Fig. 3a, b, Additional file 1). Here, three TF-2 dielectric plates with different permittivity are employed, which are 16, 4.4 and 2.2 from inside to outside. In Fig. 3c, a numerical simulation is used to evaluate the effectiveness of this discontinuous multi-layer cavity construction. Finally,

the fabricated sample, with 5.4 cm in radius and 2 cm in height (Fig. 3a inset), were constructed by precision machining of dielectric plates.

Fig. 4 Comparison of WGM in a face-shaped deformed OBH cavity and homogeneous cavity. Simulated WGM field of (**a**) deformed OBH cavity, and (**b**) deformed homogeneous cavity. White solid (dashed) curve is the deformed (circular) cavity boundary. **c** Comparison of Q-factor for a deformed OBH cavity (black curve) and homogeneous cavity (red curve) with various deformations. The resonant mode number is $m = 5$. **d** Comparison of Q-factor of deformed OBH (black curve) and homogeneous cavity (red curve) with different mode numbers

Fig. 5 WGM fields in the conformal OBH cavity and homogeneous cavity. The refractive index distribution for (**a**₁) the quadrupole OBH cavity and (**a**₂) the peanut-like OBH cavity. The maximal refractive index of quadrupole and peanut-like cavity is truncated as 27 to avoid index divergence in the core region. The typical WGM field patterns with resonant mode-number $m = 4$ of (**b**₁) the quadrupole OBH cavity and (**b**₂) the peanut-like OBH cavity. Typical WGM field patterns of (**c**₁) the homogeneous quadrupole cavity and (**c**₂) peanut-like cavity. The resonant frequency is $\sim$ 4.8 GHz and $\sim$ 7.3 GHz for quadrupole cavity and peanut-like cavity, respectively

In microwave experiments, a point source was utilized to excite the WGM, and a near-field scanning device, as illustrated in Fig. 3a, was employed to retrieve the resonant field. The scanning system was controlled by a three-axis motion controller with a sampling step of 2 mm. As comparison, a homogeneous cavity with a core of index $n'_1 = 4$ and a cladding of index $n'_0 = 2$ (6 cm in radius and 2 cm in height) was fabricated and measured. From the resonant spectra of OBH cavity (red curve) and homogeneous cavity (black curve) in Fig. 3d, the extracted Q-factor of WGM mode $m = 3$ ($m = 4$) is $\sim$ 49 ($\sim$ 241) for OBH cavity, as for homogeneous cavity, the Q-factor of WGM mode $m = 3$ ($m = 4$) is $\sim$ 25 ($\sim$ 30). The maximized Q-factor enhancement is $\sim$ 8 for mode $m = 4$, which is smaller than the simulated Q-factor enhancement of $\sim$ 12. The discrepancy between experimental and theoretical results are caused by the strong light scattering in the drilling air hole and the limited precision of mechanical machining for OBH cavity sample. Besides, the vertical radiation loss due to the air gap between samples and metal plate in the measurement also reduces

the ultimate Q-factors (Additional file 1: Fig. S7) [45]. Figure 3e plots the measured field patterns for WGM modes ($m = 3, 4$), which are in good agreement with the simulation results shown in Fig. 3f. They unambiguously demonstrate the stronger field confinement than that of the homogeneous cavity (Additional file 1: Fig. S8) [45]. Furthermore, we theoretically investigate the light trapping effect in the truncated OBH cavity. It is found that the trapped light fields are bent and directed to the inner cavity boundary and are tightly confined in the OBH cavity with clearly regular field patterns (Additional file 1: Figs. S12, S13) [45], which shows the potential of remote excitations of WGMs in OBH cavities.

In addition to demonstrating radiation Q-factor enhancement and field confinement in a circular cavity, our designed device can be generalized to the deformed cavity with directional emission [52, 53]. For example, the face-shaped cavity [25, 45] with homogeneous core and OBH cladding shows strong field confinement compared with a deformed homogeneous cavity as shown in Fig. 4a-b. In the deformed OBH cavity (Fig. 4c), the

Q-factor is increased by approximately 2 orders of magnitude. Figure 4d displays the simulated Q-factor for various resonant modes. Compared with a homogeneous deformed cavity, the Q-factor enhancement is attributed to the change of potential barrier and directional emission loss (Additional file 1: Fig. S9) [45]. Similar findings are obtained for limaçon-shaped cavities (Additional file 1: Fig. S10) [45]. Despite the fact that the expected Q-factor improvement occurs in different WGMs, there is an exceptional drop of Q-factor for the mode $m = 6$. The extraordinary optical loss is probably due to chaotic tunneling effect and requires further research [53, 54].

Furthermore, as previously suggested, using conformal mapping $w^2 = \chi^2 - 1$ for circular OBH cavity, we have obtained quadrupole OBH cavity and peanut-like (dual cores) OBH cavity with gradient index both in the core and cladding regions, as shown in Fig. 5(a_1, a_2). It can be found that WGM fields in these conformal OBH cavities (Fig. 5b_1, b_2) are tightly confined in the boundary compared with the homogeneous cavity (Fig. 5c_1, c_2). Besides, the Q-factor of conformal quadrupole cavity (peanut-like cavity) is boosted by 7 (4) orders of magnitude compared with a homogeneous one (see Additional file 1) [45]. The different Q-factor enhancement can be attributed to the various cavity structures in the virtual w-space for the conformal mapping. Given the ingenious conformal transformation, theoretically the OBH cavity with arbitrary boundary shapes can be constructed, which may provide a new avenue to cavity optics for fundamental physics and photonic applications.

3 Conclusions

In summary, we have reported a group of conformal OBH cavities based on transformation optics. The universal radiation loss in a conventional homogeneous cavity is completely inhibited in the ideal OBH cavity by an infinite wide potential barrier. The WGM fields in the OBH cavity are revealed to follow an unconventional $1/r^{\alpha}$ decay rule based on the conformal mapping. We demonstrate both the Q-factor enhancement and strongly confined WGM fields for a truncated OBH cavity in the microwave spectra. Furthermore, we show that the designed OBH cavity of circular shape can be applied to arbitrary-shaped cavities, which might find applications for chaotic photon transport and non-Hermitian physics with high-Q factor. For optical frequency band applications, the OBH cavity can be realized by using the gradient-thickness waveguide structures [37, 55] or gradient-size nanostructures [56]. Note that the absorption/scattering loss in the aforementioned platforms can be a serious issue, thus it is still challenging to realize high-Q OBH cavity in the optical frequency band.

Supplementary Information

Author contributions
QB and YZ contributed equally to this work. YZ fabricated the device and conducted the experiments. QB, J-hC, HC conducted theory and analyzed the data. HC conceived the idea and co-supervised the project with J-hC. All authors contributed to the discussion, analyzed the data, and wrote the manuscript. All authors read and approved the final manuscript.

Availability of data and materials
The other data that support the plots within this paper are available from the corresponding authors upon reasonable request.

Declarations

Competing interests
The authors declare that they have no competing interests.

Author details
[1]Institute of Electromagnetics and Acoustics and Department of Physics, College of Physical Science and Technology, Xiamen University, Xiamen 361005, China. [2]Fujian Provincial Key Laboratory of Electromagnetic Wave Science and Detection Technology, Xiamen 361005, China.

References
1. S. Spillane, T. Kippenberg, K. Vahala, Ultralow-threshold Raman laser using a spherical dielectric microcavity. Nature **415**(6872), 621–623 (2002)
2. L. He, ŞK. Özdemir, L. Yang, Whispering gallery microcavity lasers. Laser Photonics Rev. **7**(1), 60–82 (2013)
3. J. Zhu, S.K. Ozdemir, Y.-F. Xiao, L. Li, L. He, D.-R. Chen, L. Yang, On-chip single nanoparticle detection and sizing by mode splitting in an ultrahigh-Q microresonator. Nat. Photonics **4**(1), 46–49 (2010)

4.   M.R. Foreman, J.D. Swaim, F. Vollmer, Whispering gallery mode sensors. Adv. Opt. Photonics **7**(2), 168–240 (2015)

5.   N. Toropov, G. Cabello, M.P. Serrano, R.R. Gutha, M. Rafti, F. Vollmer, Review of biosensing with whispering-gallery mode lasers. Light Sci. Appl. **10**(1), 42 (2021)

6.   X. Zhang, Q.-T. Cao, Z. Wang, Y.-X. Liu, C.-W. Qiu, L. Yang, Q. Gong, Y.-F. Xiao, Symmetry-breaking-induced nonlinear optics at a microcavity surface. Nat. Photonics **13**(1), 21–24 (2019)

7.   X. Lu, G. Moille, Q. Li, D.A. Westly, A. Singh, A. Rao, S.-P. Yu, T.C. Briles, S.B. Papp, K. Srinivasan, Efficient telecom-to-visible spectral translation through ultralow power nonlinear nanophotonics. Nat. Photonics **13**(9), 593–601 (2019)

8.   J.-H. Chen, X. Shen, S.-J. Tang, Q.-T. Cao, Q. Gong, Y.-F. Xiao, Microcavity nonlinear optics with an organically functionalized surface. Phys. Rev. Lett. **123**(17), 173902 (2019)

9.   S. Haroche, J.-M. Raimond, *Exploring the Quantum: Atoms, Cavities, and Photons* (Oxford University Press, Oxford, 2006)

10. P. Lodahl, S. Mahmoodian, S. Stobbe, A. Rauschenbeutel, P. Schneeweiss, J. Volz, H. Pichler, P. Zoller, Chiral quantum optics. Nature **541**(7638), 473–480 (2017)

11. Z. Yang, M. Jahanbozorgi, D. Jeong, S. Sun, O. Pfister, H. Lee, X. Yi, A squeezed quantum microcomb on a chip. Nat. Commun. **12**(1), 4781 (2021)

12. M. Zhang, C. Wang, R. Cheng, A. Shams-Ansari, M. Lončar, Mono-lithic ultra-high-Q lithium niobate microring resonator. Optica **4**(12), 1536–1537 (2017)

13. J. Lin, N. Yao, Z. Hao, J. Zhang, W. Mao, M. Wang, W. Chu, R. Wu, Z. Fang, L. Qiao, Broadband quasi-phase-matched harmonic generation in an on-chip monocrystalline lithium niobate microdisk resonator. Phys. Rev. Lett. **122**(17), 173903 (2019)

14. C. Wang, Z. Fang, A. Yi, B. Yang, Z. Wang, L. Zhou, C. Shen, Y. Zhu, Y. Zhou, R. Bao, High-Q microresonators on 4H-silicon-carbide-on-insulator platform for nonlinear photonics. Light Sci. Appl. **10**(1), 139 (2021)

15. E.E. Narimanov, A.V. Kildishev, Optical black hole: Broadband omnidirectional light absorber. Appl. Phys. Lett. **95**(4), 041106 (2009)

16. Y.-F. Xiao, C.-L. Zou, B.-B. Li, Y. Li, C.-H. Dong, Z.-F. Han, Q. Gong, High-Q exterior whispering-gallery modes in a metal-coated microresonator. Phys. Rev. Lett. **105**(15), 153902 (2010)

17. P.J. Wyatt, Scattering of electromagnetic plane waves from inhomogeneous spherically symmetric objects. Phys. Rev. **127**(5), 1837 (1962)

18. A. Chiasera, Y. Dumeige, P. Feron, M. Ferrari, Y. Jestin, G. Nunzi Conti, S. Pelli, S. Soria, G.C. Righini, Spherical whispering-gallery-mode microresonators. Laser Photonics Rev. **4**(3), 457–482 (2010)

19. S. Spillane, T. Kippenberg, K. Vahala, K. Goh, E. Wilcut, H. Kimble, Ultra-high-Q toroidal microresonators for cavity quantum electrodynamics. Phys. Rev. A **71**(1), 013817 (2005)

20. A.B. Matsko, V.S. Ilchenko, Optical resonators with whispering-gallery modes-part i: basics. IEEE J. Sel. Top. Quantum Electron. **12**(1), 3–14 (2006)

21. K.J. Vahala, Optical microcavities. Nature **424**(6950), 839–846 (2003)

22. J. Buck, H. Kimble, Optimal sizes of dielectric microspheres for cavity QED with strong coupling. Phys. Rev. A **67**(3), 033806 (2003)

23. W. Liu, A.E. Miroshnichenko, Y.S. Kivshar, Q-factor enhancement in all-dielectric anisotropic nanoresonators. Phys. Rev. B **94**(19), 195436 (2016)

24. S. Jahani, Z. Jacob, Transparent subdiffraction optics: nanoscale light confinement without metal. Optica **1**(2), 96–100 (2014)

25. X.-F. Jiang, Y.-F. Xiao, C.-L. Zou, L. He, C.-H. Dong, B.-B. Li, Y. Li, F.-W. Sun, L. Yang, Q. Gong, Highly unidirectional emission and ultralow-threshold lasing from on-chip ultrahigh-Q microcavities. Adv. Mater. **24**(35), 260–264 (2012)

26. B. Min, E. Ostby, V. Sorger, E. Ulin-Avila, L. Yang, X. Zhang, K. Vahala, High-Q surface-plasmon-polariton whispering-gallery microcavity. Nature **457**(7228), 455–458 (2009)

27. Y. Chen, Y. Yin, L. Ma, O.G. Schmidt, Recent progress on optoplasmonic whispering-gallery-mode microcavities. Adv. Opt. Mater. **9**, 2100143 (2021)

28. U. Leonhardt, Optical conformal mapping. Science **312**(5781), 1777–1780 (2006)

29. J.B. Pendry, D. Schurig, D.R. Smith, Controlling electromagnetic fields. Science **312**(5781), 1780–1782 (2006)

30. H. Chen, C.T. Chan, P. Sheng, Transformation optics and metamaterials. Nat. Mater. **9**(5), 387–396 (2010)

31. Y. Lai, J. Ng, H. Chen, D. Han, J. Xiao, Z.-Q. Zhang, C.T. Chan, Illusion optics: the optical transformation of an object into another object. Phys. Rev. Lett. **102**(25), 253902 (2009)

32. L. Xu, H. Chen, Conformal transformation optics. Nat. Photonics **9**(1), 15–23 (2015)

33. Y. Kim, S.-Y. Lee, J.-W. Ryu, I. Kim, J.-H. Han, H.-S. Tae, M. Choi, B. Min, Designing whispering gallery modes via transformation optics. Nat. Photonics **10**(10), 647–652 (2016)

34. J. Pendry, Y. Luo, R. Zhao, Transforming the optical landscape. Science **348**(6234), 521–524 (2015)

35. R.-Q. Li, D. Hernángomez-Pérez, F. García-Vidal, A. Fernández-Domínguez, Transformation optics approach to plasmon-exciton strong coupling in nanocavities. Phys. Rev. Lett. **117**(10), 107401 (2016)

36. D. Schurig, J.J. Mock, B. Justice, S.A. Cummer, J.B. Pendry, A.F. Starr, D.R. Smith, Metamaterial electromagnetic cloak at microwave frequencies. Science **314**(5801), 977–980 (2006)

37. C. Sheng, H. Liu, Y. Wang, S. Zhu, D. Genov, Trapping light by mimicking gravitational lensing. Nat. Photonics **7**(11), 902–906 (2013)

38. S. Liu, L. Li, Z. Lin, H. Chen, J. Zi, C.T. Chan, Graded index photonic hole: Analytical and rigorous full wave solution. Phys. Rev. B **82**(5), 054204 (2010)

39. Q. Cheng, T.J. Cui, W.X. Jiang, B.G. Cai, An omnidirectional electromagnetic absorber made of metamaterials. New J. Phys. **12**(6), 063006 (2010)

40. H. Chen, S. Tao, J. Bělín, J. Courtial, R.-X. Miao, Transformation cosmology. Phys. Rev. A **102**(2), 023528 (2020)

41. W. Xiao, S. Tao, H. Chen, Mimicking the gravitational effect with gradient index lenses in geometrical optics. Photon. Res. **9**(7), 1197–1203 (2021)

42. T.G. Mackay, A. Lakhtakia, Towards a metamaterial simulation of a spinning cosmic string. Phys. Lett. A **374**(23), 2305–2308 (2010)

43. C. Sheng, H. Liu, H. Chen, S. Zhu, Definite photon deflections of topological defects in metasurfaces and symmetry-breaking phase transitions with material loss. Nat. Commun. **9**(1), 4271 (2018)

44. D.A. Genov, S. Zhang, X. Zhang, Mimicking celestial mechanics in metamaterials. Nat. Phys. **5**(9), 687–692 (2009)

45. See Supplemental Material for details

46. R.G. John Heebner, T. Ibrahim, *Optical Microresonators Theory* (Fabrication and Applications. Springer, New York, 2003)

47. B. Johnson, Theory of morphology-dependent resonances: shape resonances and width formulas. J. Opt. Soc. Am. A **10**(2), 343–352 (1993)

48. D. Zhu, Y. Zhou, X. Yu, P. Shum, F. Luan, Radially graded index whispering gallery mode resonator for penetration enhancement. Opt. Express **20**(24), 26285–26291 (2012)

49. S. Jahani, Z. Jacob, All-dielectric metamaterials. Nat. Nanotechnol. **11**(1), 23–36 (2016)

50. X. Wang, H. Chen, H. Liu, L. Xu, C. Sheng, S. Zhu, Self-focusing and the talbot effect in conformal transformation optics. Phys. Rev. Lett. **119**(3), 033902 (2017)

51. P. Moitra, Y. Yang, Z. Anderson, I.I. Kravchenko, D.P. Briggs, J. Valentine, Realization of an all-dielectric zero-index optical metamaterial. Nat. Photonics **7**(10), 791–795 (2013)

52. X. Jiang, L. Shao, S.-X. Zhang, X. Yi, J. Wiersig, L. Wang, Q. Gong, M. Lončar, L. Yang, Y.-F. Xiao, Chaos-assisted broadband momentum transformation in optical microresonators. Science **358**(6361), 344–347 (2017)

53. L.-K. Chen, Y.-Z. Gu, Q.-T. Cao, Q. Gong, J. Wiersig, Y.-F. Xiao, Regular-orbit-engineered chaotic photon transport in mixed phase space. Phys. Rev. Lett. **123**(17), 173903 (2019)

54. Y.-Z. Gu, L.-K. Chen, Y.-J. Qian, Q. Gong, Q.-T. Cao, Y.-F. Xiao, Layered localization in a chaotic optical cavity. Phys. Rev. E **102**(6), 062208 (2020)

55. T. Zentgraf, Y. Liu, M.H. Mikkelsen, J. Valentine, X. Zhang, Plasmonic luneburg and eaton lenses. Nat. Nanotechnol. **6**(3), 151–155 (2011)

56. Y. Zhang, Y. He, H. Wang, L. Sun, Y. Su, Ultra-broadband mode size converter using on-chip metamaterial-based luneburg lens. ACS Photonics **8**(1), 202–208 (2020)